RAPID COMMUNICATIONS

PHYSICAL REVIEW B VOLUME 47, NUMBER 7 15 FEBRUARY 1993-I

Observation of the interfacial-field-induced weak antilocalization in InAs quantum structures

G. L. Chen, J. Han, T. T. Huang, S. Datta, and D. B. Janes
School of Electrical Engineering, Purdue University, West Lafayette, Indiana 47907
(Received 30 November 1992)

We have studied low-temperature magnetoconductance and observed weak antilocalization in an AlSb/InAs/AlSb quantum-well structure. The spin-orbital field deduced from the antilocalization data is found to be insensitive to photoinduced changes in the carrier density, suggesting that the interfacial-field-induced rather than the crystal-field-induced spin splitting is the predominant cause of the spin-orbital scattering. We also find a significant enhancement of spin-orbital scattering in ZnTe/InAs/AlSb structures which can be explained by the structural asymmetry, thereby confirming the dominant role of the interfacial field.

Weak localization comes from the constructive interference of two time-reversed paths of a conduction electron in a disordered system and results in the quantum reduction of conductance. However, in the presence of strong spin dephasing, i.e., the electron changing spin direction during conduction, the two time-reversed paths, experiencing reversed spin-dephasing processes, give rise to destructive interference and enhance the conductance instead; this is referred to as weak antilocalization.[1] Since an external magnetic field destroys the spatial phase coherence of the two paths, one observes positive (negative) magnetoconductance at low fields as the signature of the weak localization (antilocalization). Antilocalization has been extensively studied in metal films.[2] It is understood that the spin-orbital scattering from impurities, especially heavy impurities, causes the spin dephasing in these systems. Antilocalization in semiconductor two-dimensional electron gases (2DEG) has also been observed.[3,4] Kawaguchi, Takayanagi, and Kawaji observed antilocalization behavior in InAs metal-oxide-semiconductor inversion layers; yet the mechanism was not well understood.[5] Recently Dresselhaus *et al.*[6] reported the observation of antilocalization in GaAs inversion layers and attributed the spin dephasing to the randomized spin precession processes which were first described by D'yakanov and Perel'[7] (DP), and further identified the cause as the crystal-field-induced spin splitting.

There are two major sources of the electric fields that cause the spin splitting. One is the crystal field due to the inversion asymmetry of the zinc-blende structure which we will refer to as the I term;[8] the other is the confining electric field of the quantum structure, known as the Rashba term (the R term).[9] In this paper, we report the observation of pronounced antilocalization behavior in the AlSb/InAs/AlSb quantum well and ZnTe/InAs/AlSb quantum structures. Our results can be understood in terms of the DP mechanism. However, the observed enhancement of spin dephasing by structural asymmetry, along with the carrier density dependence studies suggests that in our structures it is the interfacial Rashba field rather than the crystal field that causes the spin dephasing.

The nonintentionally doped AlSb/InAs/AlSb and ZnTe/InAs/AlSb structures were grown by molecular-beam epitaxy. The ZnTe/InAs/AlSb structures are developed to implement field-effect transistors and the detailed growth information is given in a separate publication,[10] while the AlSb/InAs/AlSb structure is similar to those described in the literature.[11] We have investigated three samples (samples $A-C$) for spin-orbital scattering, of which samples A and C have the AlSb/InAs/AlSb and ZnTe/InAs/AlSb structures, respectively. Sample B also has a ZnTe/InAs/AlSb configuration; however, two AlSb monolayers are incorporated at the ZnTe/InAs interface, making the structure intermediate between ZnTe/InAs/AlSb and AlSb/InAs/AlSb structures. The thicknesses of the InAs layers in samples $A-C$ were measured to be 150, 125, and 150 Å, respectively, by transmission electron microscopy. A 1.0-mm-long and 0.15-mm-wide Hall bar was photolithographically defined and etched for each sample. Contacts to the 2DEG's were implemented by depositing indium dots on the film surface with a hot (370 °C) solder tip. Low-temperature resistance was measured in a ^{4}He cryostat by using a Linear Research LR4000 AC lock-in bridge operated at 17 Hz. Excitation was kept low to avoid heating effects. Magnetoresistance up to 8 T and Hall measurements were performed and single-frequency Shubunikov–de Haas (SdH) oscillations were observed in all the samples. We also observed quantum Hall effect in samples A and B.

Low-field negative magnetoconductance of sample A at 4.2 K is shown in Fig. 1. The experimental data are fit with the 2D weak localization magnetoconductance formula[2]

$$\Delta g(H)=\frac{-e^2}{2\pi^2\hbar}\left\{\Psi\left[\frac{1}{2}+\frac{H_1}{H}\right]-\Psi\left[\frac{1}{2}+\frac{H_2}{H}\right]+\frac{1}{2}\left[\Psi\left[\frac{1}{2}+\frac{H_3}{H}\right]-\Psi\left[\frac{1}{2}+\frac{H_2}{H}\right]\right]\right\}. \quad (1)$$

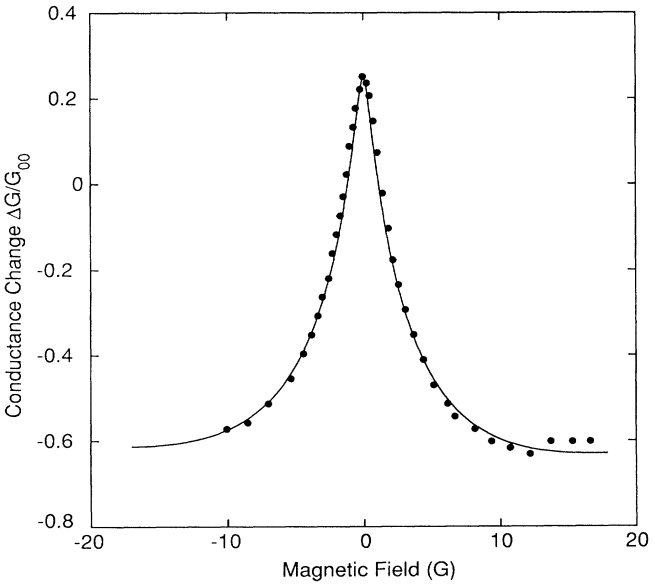

FIG. 1. Magnetoconductance of sample A at 4.2 K. The solid curves are the fit of the experimental data to Eq. (1). $G_{00}=e^2/2\pi^2\hbar\approx 1.23\times 10^{-5}\ \Omega^{-1}$.

Here Δg is the quantum correction to conductance, and Ψ is the digamma function, the effective fields are defined by $H_1=H_e+H_{so}+H_s$, $H_2=H_i+\frac{4}{3}H_{so}+\frac{2}{3}H_s$, $H_3=H_i+2H_s$, and $H_\alpha=\hbar/4De\tau_\alpha$, D being the diffusivity, given by $\frac{1}{2}v_F^2\tau_e$, τ_α's being the characteristic transport times, and the α's correspond to elastic (e), inelastic (i), spin-orbital (so), or spin-spin (s). Antilocalization occurs when spin dephasing is strong, i.e., $\tau_{so}<\tau_i$. Here we follow the usual notations of weak localization theories by using τ_{so}, even though the spin-dephasing processes in our samples do not originate from impurity related spin-orbital scattering. In the simulations, we assume no magnetic impurities in the system, therefore $H_s=0$. τ_i and τ_{so} are the only two parameters in the curve fitting. Simulations show that the negative magnetoconductance curve saturates at $\sim 4H_{so}$, when $\tau_{so}\ll\tau_i$.

Unlike the well-known spin-orbital scattering in metal films, where the spin-orbital coupling is associated with the electric field of an impurity,[12] the DP spin-dephasing mechanism is affiliated with the dipole field due to inversion asymmetry (the I term) or the interfacial field (the R term). Analogous to spin-orbital interaction, the electric field transforms into an effective magnetic field in the moving frame of the conduction electron and causes the spin splitting ΔE_c in the conduction band. At the same time, this magnetic field, directed perpendicular to the motion, causes the spin to precess around the field direction with frequency $\Omega=\Delta E_c/2\hbar$. In the presence of elastic scattering, when $\tau_e^{-1}>\Omega$, the electron scatters before it reaches an eigenstate of the system. Each scattering event changes the direction of the effective magnetic field which depends on the electron wave vector and causes the electron to precess around a new direction, thus randomizing the precession process.[7,13] This is analogous to the motional narrowing in electron-spin resonance,[14] giving a spin-dephasing rate

$$\tau_{so}^{-1}=\langle \Delta E_c^2\rangle \tau_e/4\hbar^2 . \tag{2}$$

Here $\langle \Delta E_c^2\rangle$ is the Fermi-surface average of ΔE_c^2 and τ_{so} is inversely proportional to τ_e due to the randomization.

Theoretical calculations show that the I term is much larger than the R term in wide-band-gap material quantum structures, such as GaAs inversion layers. The calculations also predict that the R term increases much faster than the I term as the band gap becomes smaller, and therefore the R term is expected to be more significant in narrow-band-gap materials.[15] One way to distinguish the two terms is to study their different forms of carrier density dependence. Due to the different physical origins of the electric fields, the spin splitting of the two terms depends on the wave vector k differently. ΔE_c of the I term has k^3 dependence, while that of the R term has linear k dependence.[15,16] Using Eq. (2) and the definition of H_{so}, we find the quadratic dependence of spin-orbital field H_{so} on carrier density N_s for the I term,

$$H_{so}=\eta N_s^2 , \tag{3}$$

while H_{so} is independent of N_s for the R term,

$$H_{so}=\gamma\langle E_z\rangle^2 . \tag{4}$$

Here $\langle E_z\rangle$ is the expectation value of the electric field perpendicular to the film surface, while η and γ are constants independent of carrier density.

We used red light-emitting diodes (LED's) ($\lambda\approx 655$ nm) to change the 2DEG carrier density in sample A. To ensure more uniform illumination, the LED's were wrapped with filter paper. Negative photoconductivities were observed,[11] and both the Hall measurement and the change of SdH oscillation frequency showed the decrease of the carrier density under illumination. In the experiment, we were able to change the density by $\sim 20\%$. The density dependence of H_{so} is shown in Fig. 2, where the dashed and solid lines are predictions of Eqs. (3) and (4), respectively. The fact that the data do not follow the quadratic dependence (dashed line) clearly excludes the predominance of the I term. Meanwhile the data show that H_{so} are essentially independent of carrier density. This fits well with the prediction of the R term, if one assumes that $\langle E_z\rangle$ does not change significantly under the photoinduced carrier density change within the experimental range.

As stated in Eq. (4), the spin-orbital field is proportional to the square of the expectation value of the interfacial field $\langle E_z\rangle$, which is commonly zero for a bound state, causing the interfacial-field-induced spin-orbital scattering to vanish. However, it is pointed out by Lommer, Malcher, and Rössler[15] that $\langle E_z\rangle$ is nonzero in heterostructures, where different material layers have different effective masses. In addition to nonuniform mass, structural asymmetry is also essential to have nonzero $\langle E_z\rangle$. In a perfectly symmetric well, $\langle E_z\rangle$ is identically zero. On the other hand, $\langle E_z\rangle$ is enhanced by introducing asymmetry into the structure.

Starting from a 1D Schrödinger equation in the case

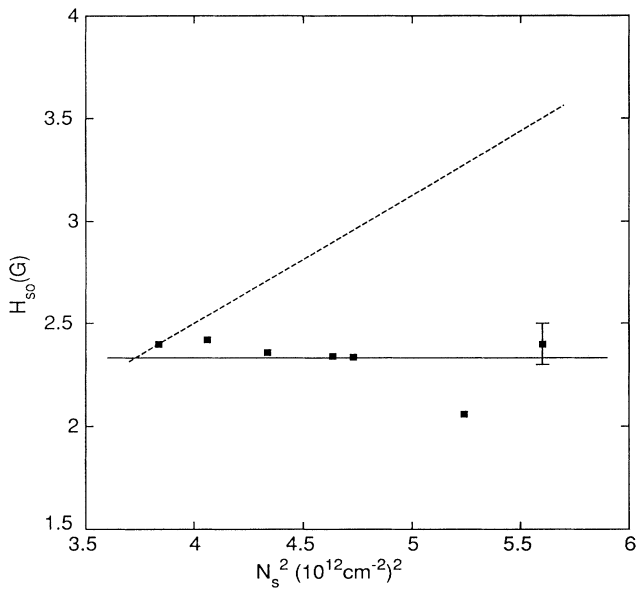

FIG. 2. Spin-orbital field H_{so} vs 2DEG carrier density N_s. The dashed line is the prediction of Eq. (3), taking the leftmost data point as the reference. The flat solid line, taking the average value of all the data points, is drawn according to Eq. (7). The error bar depicts the average error tolerance of all the data points in fitting the antilocalization curves, as shown in Fig. 1.

that effective mass changes with position,

$$-(\hbar^2/2)(d/dz)(m^{-1}d\psi/dz)+V\psi=E\psi\ , \tag{5}$$

we can show that for a bound state

$$\langle E_z\rangle=-\langle\psi|dV/dz|\psi\rangle$$
$$=(\hbar^2/2)\int_{-\infty}^{\infty}(m^{-1}d\psi/dz)^2(dm/dz)dz\ . \tag{6}$$

Obviously, $\langle E_z\rangle$ becomes zero when effective mass is constant. It is instructive to apply Eq. (6) to some simple structures, as shown in Fig. 3. It is easy to see that $\langle E_z\rangle$ is nonzero in (a) and (b), while $\langle E_z\rangle$ is suppressed by symmetry and vanishes in (c).

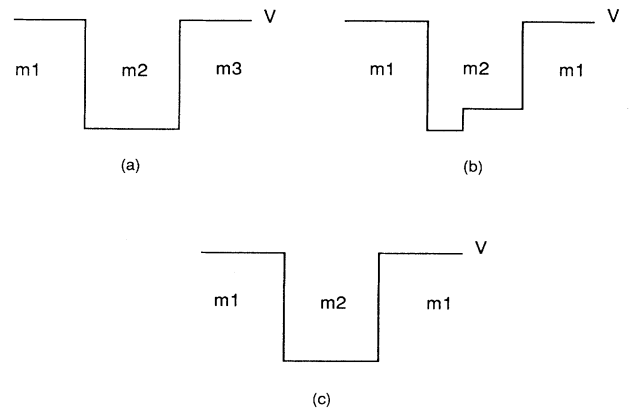

FIG. 3. Three simple 1D heterostructure quantum-well models to illustrate the asymmetry effect on $\langle E_z\rangle$. $\langle E_z\rangle\neq 0$ in asymmetric structure (a) and (b), while $\langle E_z\rangle=0$ in symmetric structure (c). $m1\neq m2\neq m3$.

Following the symmetry arguments above, we expect enhancements of spin-orbital scattering in samples B and C, which have the ZnTe/InAs/AlSb structures. Figures 4(a) and 4(b) show the magnetoconductance of samples B and C at 4.2 K, respectively. The negative magnetoconductance curves of samples $A-C$ are similar in shape, but each curve has a different magnetic-field scale. The spin-orbital scattering enhancement from sample A to C is very significant, while sample B, being intermediate in terms of structural asymmetry, has the intermediate spin-orbital scattering strength. Transport parameters of

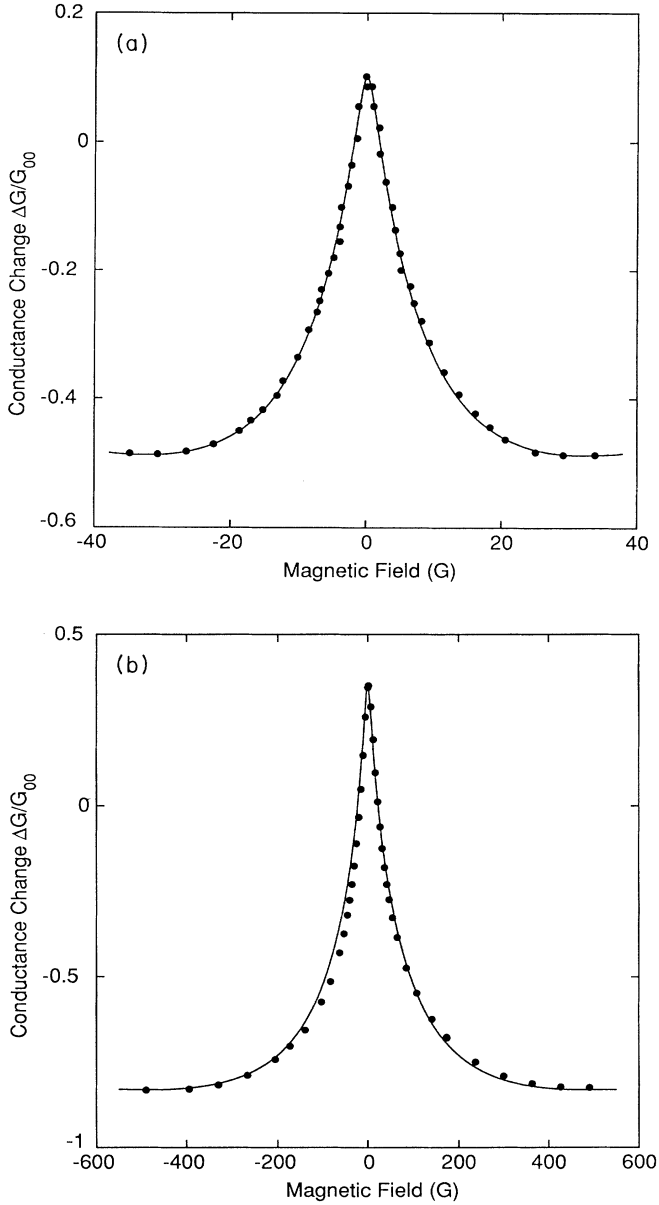

FIG. 4. Magnetoconductance of (a) sample B and (b) sample C at 4.2 K. The solid curves are the fit of the experimental data to Eq. (1). Notice that the field scales on (a) and (b) are different.

TABLE I. Transport parameters of samples $A-C$ at 4.2 K. Values of carrier density N_s, mobility μ, and elastic scattering time τ_e are directly measured from experiment. Spin-dephasing time τ_{so} is deduced from curve fitting, and values of spin-orbital field H_{so} and spin-splitting energy ΔE_c are thereby calculated.

Sample	Structure	Mobility ($cm^2/V\,s$)	Density (10^{12} cm^{-2})	τ_e (ps)	τ_{so} (ps)	H_{so} (G)	$\langle \Delta E_c^2 \rangle$ (meV^2)
A	AlSb/InAs/AlSb	2.77×10^4	2.37	0.630	1.75	2.4	1.57
B	ZnTe/(AlSb)/InAs/AlSb	1.27×10^4	2.74	0.360	1.65	5.98	2.92
C	ZnTe/InAs/AlSb	4.27×10^3	3.91	0.129	0.32	68	42

the three samples are summarized in Table I for comparison.

Due to the different effective masses of ZnTe, InAs, and AlSb materials, the ZnTe/InAs/AlSb configuration has the asymmetry illustrated in Fig. 3(a). The AlSb/InAs/AlSb configuration has the same barrier material at both sides of the well; however, the quantum well has a nonflat well bottom due to nonuniform charging effect, and therefore can be modeled as Fig. 3(b). Using these simple models we estimate that the mean value of the field $\langle E_z \rangle$ is 1.5×10^6 V/m for sample *A* and 1.9×10^7 for sample *C*. For comparison, the experimental values are found to be 2.60×10^6 V/m for sample *A* and 1.19×10^7 V/m for sample *C*, according to Eq. (4) in which the constant γ can be determined by following the procedures described in Ref. 15. The simple models estimate $\langle E_z \rangle$ at the right order of magnitude and demonstrate the correct asymmetry trend as well. Since $\langle E_z \rangle$ is largely determined by asymmetry, it is not surprising to see that 20% reduction in carrier density does not change $\langle E_z \rangle$ significantly in the carrier density dependence study. We simulate the band diagram of sample *A* by solving the Poisson equation numerically,[17] and find that 20% change in carrier density does little in changing the quantum-well profile.

In conclusion, weak antilocalization behavior is observed in both AlSb/InAs/AlSb and ZnTe/InAs/AlSb quantum structures. We have studied the carrier density dependence and observed the significant enhancement of spin dephasing by asymmetry. Our studies suggest the predominance of the asymmetric interfacial Rashba field in InAs quantum structures.

The authors would like to thank M. P. Young and Y. Fan for technical assistance and P. Bagwell, B. Das, J. Liu, and N. Giordano for helpful discussions. In particular, we are grateful to Professor R. Reifenberger for allowing us to use his Hall measurement apparatus, and Professor R. L. Gunshor for his assistance in film growth. This work was supported by National Science Foundation Division of Materials Research Grant No. DMR-89-13706.

[1]S. Hikami, A. I. Larkin, and Y. Nagaoka, Prog. Theor. Phys. **63**, 707 (1980).

[2]For a review article on weak localization in metal films, see G. Bergmann, Phys. Rep. **107**, 1 (1984).

[3]D. A. Poole, M. Pepper, and A. Hughes, J. Phys. C **15**, L1137 (1982).

[4]S. Kawaji, K. Kuboki, H. Shigeno, T. Nambu, J. Wakabayashi, J. Yoshino, and H. Sakaki, in *Proceedings of the 17th International Conference on the Physics of Semiconductors,* edited by J. D. Chadi and W. A. Harrison (Springer-Verlag, Berlin, 1985), p. 413.

[5]Y. Kawaguchi, I. Takayanagi, and S. Kawaji, J. Phys. Soc. Jpn. **56**, 1293 (1987).

[6]P. D. Dresselhaus, C. M. A. Papavassiliou, R. G. Wheeler, and R. N. Sacks, Phys. Rev. Lett. **68**, 106 (1992).

[7]M. I. D'yakanov and V. I. Perel', Zh. Eksp. Teor. Fiz. **60**, 1954 (1971) [Sov. Phys. JEPT **33**, 1053 (1971)].

[8]G. Dresselhaus, Phys. Rev. **100**, 580 (1955); L. M. Roth, *ibid.* **173**, 755 (1968).

[9]Y. A. Bychkov and E. I. Rashba, J. Phys. C **17**, 6039 (1984).

[10]J. Han, T. S. Stavrinides, R. L. Gunshor, and M. Kobayashi (unpublished).

[11]G. Tuttle, H. Kroemer, and J. H. English, J. Appl. Phys. **65**, 5239 (1989).

[12]R. J. Elliott, Phys. Rev. **96**, 266 (1954).

[13]A. H. Clark, R. D. Burnham, D. J. Chadi, and R. M. White, Phys. Rev. B **12**, 5758 (1975).

[14]C. Kittel, *Introduction to Solid State Physics,* 4th ed. (Wiley, New York, 1971), p. 586.

[15]G. Lommer, F. Malcher, and U. Rössler, Phys. Rev. B **32**, 6965 (1985); Phys. Rev. Lett. **60**, 728 (1988).

[16]B. Das, S. Datta, and R. Reifenberger, Phys. Rev. B **41**, 8278 (1990).

[17]M. S. Lundstrom and R. J. Schuelke, Solid State Electron. **25**, 683 (1982).